Vibration Characteristics for Piezoelectric Cylinders Using Amplitude-Fluctuation Electronic Speckle Pattern Interferometry

Chi-Hung Huang* and Chien-Ching Ma†

National Taiwan University, Taipei 10617, Taiwan, Republic of China

Electronic speckle pattern interferometry (ESPI) is a full-field, noncontact technique for measuring the deformation of a structure subjected to static loading or, especially, to dynamic vibration. Three-dimensional vibrations of piezoelectric materials with cylindrical surfaces are investigated using the amplitude-fluctuation ESPI (AF-ESPI) method. This method demonstrates the advantages of combining noise reduction, like the subtraction method, and high fringe sensitivity, like the time-averaged method. The optical system for AF-ESPI with two in-plane and one out-of-plane measurements is employed to study the volume vibration of a piezoelectric material for a thick circular disk, a ring, and a thin-walled tube. Because the clear fringe patterns measured by the AF-ESPI method will be shown only at resonant frequencies, both the resonant frequencies and the complete vibration mode shapes in three dimensions are obtained experimentally. Finally, impedance analysis and the finite element method are also utilized, and the results are compared with the measurements obtained by AF-ESPI. It is shown that the numerical calculations and the experimental results agree fairly well for both the resonant frequencies and the mode shapes in three-dimensional configurations.

I. Introduction

WHEN a coherent laser beam illuminates a rough surface, we can observe the curious granular appearance of such a surface. This is known as the speckle effect. The speckle effect is no longer looked upon as only noise but also as an information carrier, which can be used in many applications. The sensitivity of the speckle method is controlled by the size of speckles, which is the resolution limit of the speckle method. Making use of a standard television camera to digitize the speckles and to record the fringe patterns eliminates the use of photographic film. This method is known as electronic speckle pattern interferometry (ESPI).

ESPI is a full-field, noncontact, and real-time measurement method of deformation for structures subjected to various kinds of loadings. As compared with conventional film recording and optical reconstruction procedures used for holographic interferometry,[1] the interferometric fringe patterns of ESPI can be displayed directly in a video monitor. The comparative advantage of operation allows ESPI to extend its application compared with other optical measurement techniques. ESPI was first proposed by Butters and Leendertz,[2] who investigated the out-of-plane measurement of a vibrating disk. The most widely used experimental setup to study dynamic responses by ESPI is the time-averaged vibration ESPI method.[3] The disadvantage of this method is that the interferometry fringes represent the amplitude but not the phase of the vibration. To improve this shortcoming, the phase-modulation method, using the reference beam modulation technique, was developed to determine the relative phase of displacement.[4,5] Shellabear and Tyrer[6] used ESPI to make three-dimensional vibration measurements. Three different illumination geometries were constructed, and the orthogonal components of vibration amplitude and mode shape were determined. To reduce the noise coming from the environment, the subtraction method was developed.[7,8] The subtraction method differs from the time-averaged method in that the reference frame is recorded before vibration and is continuously subtracted from the incoming frames after vibration. However, the interferometric fringe visibility of the subtraction method is not good enough for quantitative

measurement. To increase the visibility of the fringe pattern and to reduce the environmental noise simultaneously, an amplitude-fluctuation ESPI method was proposed by Wang et al.[9] for out-of-plane vibration measurement. In the amplitude-fluctuation ESPI method, the reference frame is recorded in a vibrating state and subtracted from the incoming frame. Consequently, it combines the advantages of the time-averaged and subtraction methods, i.e., good visibility and noise reduction.

Since Pierre and Jacques Curie discovered the piezoelectric effect in 1880, there had been a large amount of research and applications,[10,11] such as piezoelectric actuators, ultrasonic motors, nondestructive testing devices, etc. Piezoelectricity describes the phenomenon that the material induces an electric charge when subjected to stress and, conversely, induces strain when the electric field is applied. Although the behavior of piezoelectric material can be determined by linear piezoelasticity, the Maxwell equations, piezoelectric constitutive equations, and the boundary,[12] it is difficult to obtain the analytical solutions even for a simple geometry.

In general, there are two numerical methods that are usually used to study the vibrating problem of piezoelectric materials; one is the variational approximation method, and the other is finite element analysis. Eer Nisse[13] applied the calculus of variation to the analysis of piezoelectric disks, and the solutions were compared with the experimental results obtained by Shaw.[14] Kharouf and Heyliger[15] used the Rayleigh–Ritz method to solve static and axisymmetric vibration problems for piezoelectric disks, hollow cylinders, and composite cylinders. The variation method is a powerful and accurate technique for simple geometries, and the finite element method (FEM) is an alternative method for the analysis of piezoelectric material in various complicated configurations. Kunkel et al.[16] studied the vibration modes of PZT-5H ceramics disks as regards the diameter-to-thickness D/T ratio ranging from 0.2 to 10. Guo et al.[17] presented the results for PZT-5A piezoelectric disks with D/T of 20 and 10. Adelman and Stavsky[18] derived electroelastic equations for solving the axisymmetric vibrations of radially polarized piezoelectric homogeneous ceramics tubes. Influences coming from boundary conditions and the ratio of inner/outer radii are discussed in detail. They then extended the method to study the problems of radially polarized composite piezoelectric cylinders and disks.[19]

In addition to variational and numerical methods, experimental techniques have been employed for investigating vibration modes and natural frequencies of piezoelectric transducers. Shaw[14] used an optical interference technique in which a stroboscopically

*Graduate Student, Department of Mechanical Engineering.
†Professor, Department of Mechanical Engineering.

illuminated multiple beam is applied to measure the surface motion of thick barium titanate disks. Chang[20] employed dual-beam speckle interferometry to measure the in-plane displacement.

In this paper, we employ the optical method based on amplitude-fluctuation ESPI (AF-ESPI) to study the three-dimensional vibration of piezoelectric material of a thick disk and ring that are axially polarized. In addition, a thin-walled tube with radial polarization is discussed. The advantage of using AF-ESPI is that both the resonant frequency and the corresponding vibration mode are determined experimentally. The numerical FEM with a three-dimensional model and an experimental impedance analysis is also used to study the problem, and the results are compared with those of the AF-ESPI method. It is shown that the resonant frequency difference between AF-ESPI and impedance analysis is smaller than that between AF-ESPI and the FEM.

II. Theory of AF-ESPI for Out-of-Plane and In-Plane Vibration Measurements

A. Out-of-Plane Vibration

The optical system of the ESPI setup for out-of-plane vibrating measurement is shown by Ma and Huang.[21] After the specimen vibrates, the light intensity of the reference image detected by a charge-coupled device (CCD) camera can be expressed by the time-averaged method as

$$I_1 = \frac{1}{\tau} \int_0^\tau \left\{ I_A + I_B + 2\sqrt{I_A I_B} \right.$$
$$\left. \times \cos\left[\phi + \frac{2\pi}{\lambda}(1 + \cos\theta)A\cos\omega t \right] \right\} dt \quad (1)$$

where

I_A = object light intensity
I_B = reference light intensity
τ = CCD refreshing time
ϕ = phase difference between object and reference light
λ = wavelength of laser
θ = angle between object light and observation direction
A = vibration amplitude
ω = angular frequency

Let $\Gamma = (2\pi/\lambda)(1 + \cos\theta)$ and $\tau = 2m\pi/\omega$, where m is an integer. Then Eq. (1) can be worked out as

$$I_1 = I_A + I_B + 2\sqrt{I_A I_B}(\cos\phi)J_0(\Gamma A) \quad (2)$$

where J_0 is a zero-order Bessel function of the first kind.

After image processing and rectifying, the intensity of the first image can be expressed as

$$I_1 = I_A + I_B + 2\sqrt{I_A I_B}|(\cos\phi)J_0(\Gamma A)| \quad (3)$$

As the vibration of the specimen goes on, we assume that the vibration amplitude has changed from A to $A + \Delta A$. The light intensity of the second image can be represented as

$$I_2 = \frac{1}{\tau} \int_0^\tau \{I_A + I_B + 2\sqrt{I_A I_B}\cos[\phi + \Gamma(A + \Delta A)\cos\omega t]\} dt \quad (4)$$

Expanding Eq. (4) using Taylor series expansion and neglecting the higher-order terms, we rewrite Eq. (4) as follows:

$$I_2 = I_A + I_B + 2\sqrt{I_A I_B}(\cos\phi)\left[1 - \tfrac{1}{4}\Gamma^2(\Delta A)^2\right]J_0(\Gamma A) \quad (5)$$

By image processing and rectifying, I_2 can be similarly expressed as

$$I_2 = I_A + I_B + 2\sqrt{I_A I_B}\left|(\cos\phi)\left[1 - \tfrac{1}{4}\Gamma^2(\Delta A)^2\right]J_0(\Gamma A)\right| \quad (6)$$

When these two images (the first and second images) are subtracted by the image processing system, i.e., Eq. (3) is subtracted

from Eq. (6), and are rectified, the resulting image intensity can be expressed as[21]

$$I = I_2 - I_1$$
$$= \frac{\sqrt{I_A I_B}}{2}\left|(\cos\phi)\Gamma^2(\Delta A)^2 J_0(\Gamma A)\right| \quad (7)$$

B. In-Plane Vibration

The optical setup of the system for in-plane vibration measurement is shown by Ma and Huang.[21] Similar to the out-of-plane vibration case, the first and second image intensities, i.e., I_1 and I_2, for in-plane vibration using the time-averaged method are expressed as

$$I_1 = I_A + I_B + 2\sqrt{I_A I_B}|(\cos\phi)J_0(\Gamma'A')| \quad (8)$$

$$I_2 = I_A + I_B + 2\sqrt{I_A I_B}|(\cos\phi)\left[1 - \tfrac{1}{4}\Gamma'^2(\Delta A')^2\right]J_0(\Gamma'A')| \quad (9)$$

where I_A and I_B are as earlier defined and

A' = vibration amplitude of in-plane vibration
Γ' = $(2\pi/\lambda)(2\sin\theta')$
θ' = half of the angle between two illumination lights

Subtracting Eq. (9) from Eq. (8) and rectifying by the image processing system, we can obtain the image intensity as[21]

$$I = I_2 - I_1$$
$$= \frac{\sqrt{I_A I_B}}{2}\left|(\cos\phi)\Gamma'^2(\Delta A')^2 J_0(\Gamma'A')\right| \quad (10)$$

From Eqs. (7) and (10), we find that both the out-of-plane and in-plane vibration fringe patterns obtained by the AF-ESPI method are dominated by a zero-order Bessel function J_0. The advantages for the proposed AF-ESPI method compared with the conventional subtraction method are discussed in detail by Ma and Huang.[21] Combining the out-of-plane with two in-plane optical setups by the AF-ESPI method, we can construct three-dimensional vibration characteristics of the piezoelectric material, including resonant frequencies and mode shapes at the same time. This is different from the impedance analysis, which has been used widely in determining only the resonant frequency for piezoelectric material.

III. Experimental and Numerical Results

The vibration of piezoelectric material is electroelastic in nature, and it is necessary to include the coupled electrical field with the elastic behavior. In other words, the equation of linear elasticity is coupled to the charge equation of electrostatics using the piezoelectric constants. The system of equations that governs the behavior of the vibration characteristics of piezoelectric material is presented in detail by Tiersten.[12] The linear piezoelectric constitute equations are

$$\tau_{ij} = c_{ijkl}^E s_{kl} - e_{kij}E_k, \qquad D_i = e_{ikl}s_{kl} + \varepsilon_{ik}^S E_k \quad (11)$$

where τ_{ij}, D_i, s_{ij}, and E_j represent the stress, electric displacement, strain, and electric field, respectively; and c_{ijkl}^E, e_{kij}, and ε_{ik}^S are the elastic, piezoelectric, and dielectric constants, respectively. Because of the symmetry, in general, the compressed matrix notation is introduced in place of the tensor notation. This matrix notation consists of replacing ij or kl by p or q, where i, j, k, and l take the values 1, 2, 3 and p and q take the values 1–6. By virtue of the transformation, we can make the identifications

$$c_{ijkl}^E \equiv c_{pq}^E, \qquad e_{ikl} \equiv e_{iq}, \qquad \tau_{ij} \equiv T_p \quad (12)$$

and the constitute equations (11) can be rewritten as

$$T_p = c_{pq}^E S_q - e_{kp}E_k, \qquad D_i = e_{iq}S_q + \varepsilon_{ik}^S E_k \quad (13)$$

where $s_{kl} = S_q$ when $k = l$ and $q = 1, 2, 3$ and $2s_{kl} = S_q$ when $k \neq l$ and $q = 4, 5, 6$.

Because the polarized piezoelectric ceramics have the same symmetry as a hexagonal crystal, which can be modeled as a transversely
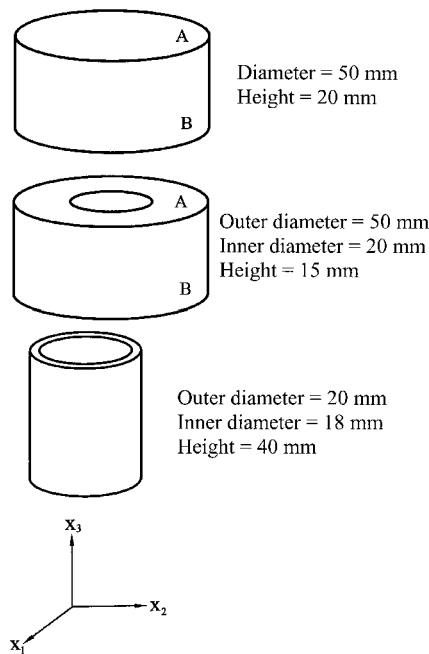
Fig. 1 Geometric dimensions and configurations of the circular disk, circular ring, and thin-walled tube.

Table 1   Material properties of PIC-151

Quantity	PIC-151
c_{11}^E, 10^{10} N/m^2	10.76
c_{33}^E	10.04
c_{12}^E	6.312
c_{13}^E	6.385
c_{44}^E	1.962
$c_{66}^E = (c_{11}^E - c_{12}^E)/2$	2.224
e_{31}, N/Vm	−9.6
e_{33}	15.1
e_{15}	12.0
$\varepsilon_{11}^S/\varepsilon_0$	1110
$\varepsilon_{33}^S/\varepsilon_0$	852
ρ, kg/m^3	7760
$\varepsilon_0 = 8.85 \times 10^{-12}$ F/m	

isotropic material, the elastic, piezoelectric, and dielectric constants are represented in matrix form as

$$c_{ij}^E = \begin{bmatrix} c_{11}^E & c_{12}^E & c_{13}^E & 0 & 0 & 0 \\ c_{12}^E & c_{11}^E & c_{13}^E & 0 & 0 & 0 \\ c_{13}^E & c_{13}^E & c_{33}^E & 0 & 0 & 0 \\ 0 & 0 & 0 & c_{44}^E & 0 & 0 \\ 0 & 0 & 0 & 0 & c_{44}^E & 0 \\ 0 & 0 & 0 & 0 & 0 & \dfrac{c_{11}^E - c_{12}^E}{2} \end{bmatrix} \quad (14)$$

$$e_{ip} = \begin{bmatrix} 0 & 0 & 0 & 0 & e_{15} & 0 \\ 0 & 0 & 0 & e_{15} & 0 & 0 \\ e_{31} & e_{31} & e_{33} & 0 & 0 & 0 \end{bmatrix} \quad (15)$$

$$\varepsilon_{ij}^S = \begin{bmatrix} \varepsilon_{11}^S & 0 & 0 \\ 0 & \varepsilon_{11}^S & 0 \\ 0 & 0 & \varepsilon_{33}^S \end{bmatrix} \quad (16)$$

Because of their wide application in precision mechanics and ultrasonics, piezoelectric materials with cylindrical shapes are selected for experimental and numerical investigations. The three types of cylindrical specimens that will be discussed in the analysis are a thick circular disk, a ring, and a thin-walled tube. The piezoelectric materials are made of Pb(Zr · Ti)O$_3$ ceramics, and the modal number is PIC-151 (Germany Physik Instrumente Company). The electroelastic properties and geometric dimensions of the specimens are shown in Table 1 and Fig. 1, respectively. The polarization direction of the circular disk and of the ring is axial, and the top and bottom surfaces are covered with silver electrodes. However, the polarization direction of the thin-walled tube is radial, and the inner and outer surfaces are covered with silver electrodes.

To measure the three independent components of displacement for volume vibrations, one out-of-plane and two in-plane ESPI systems are arranged to perform the experimental measurement. The technique of AF-ESPI for out-of-plane and in-plane vibration measurements presented in the preceding section is still applicable for cylindrical surfaces provided that the assumption of the plane wave of light beams is satisfied. The plane of the CCD camera is chosen to coincide with the Cartesian coordinate x_2–x_3 plane, as shown in
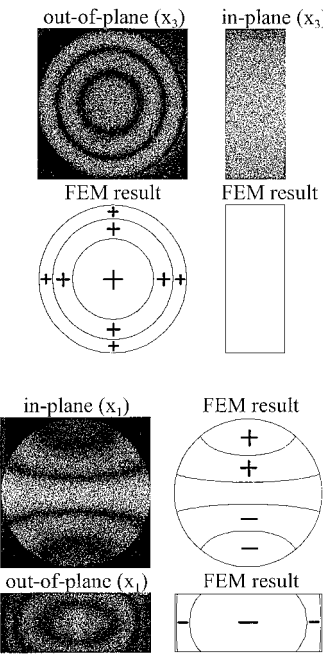

Fig. 2   First mode shape of the circular disk obtained by AF-ESPI and FEM.

Fig. 1, and the x_1 axis is in the normal direction. The out-of-plane optical system used will measure the displacement component along the x_1 direction of the cylindrical surface. Hence, displacements of the cylindrical surface measured by the out-of-plane setup consist of displacements along the radial and angular directions. Similarly, the two in-plane setups will measure the displacement magnitudes in the x_2 and x_3 directions. However, the regions of the two light beams overlap, which causes the interferometry, and the focus plane of the CCD camera cannot cover the entire cylindrical surface; hence, the clarity and the resolution of fringe patterns are not as good as that for plane surfaces.

A 30-mW He–Ne laser with wavelength $\lambda = 632.8$ nm is used as the coherent light source. We use a CCD camera (Pulnix Company) and a P360F (Dipix Technologies, Inc.) frame grabber with a digital signal processor onboard to record and process the images. To achieve the sinusoidal output, a function generator HP33120A (Hewlett Packard) connected to a 4005 power amplifier (NF Corporation) is used. Because the electrical impedance of the piezoelectric transducer drops to a local minimum when it vibrates at a resonant frequency, the resonant frequency can also be determined by impedance analysis, and it is carried out by using an HP4194A impedance/gain-phase analyzer (Hewlett Packard). Numerical results of resonant frequencies and mode shapes are calculated by the ABAQUS finite element package[22] in which 20-node three-dimensional brick elements (C3D20E) are selected to analyze the problem. Both the experimental measurements obtained
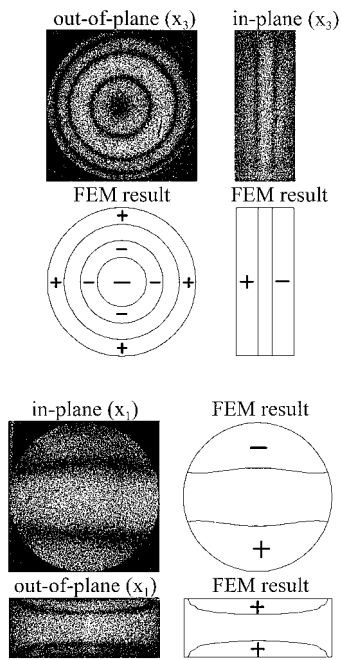
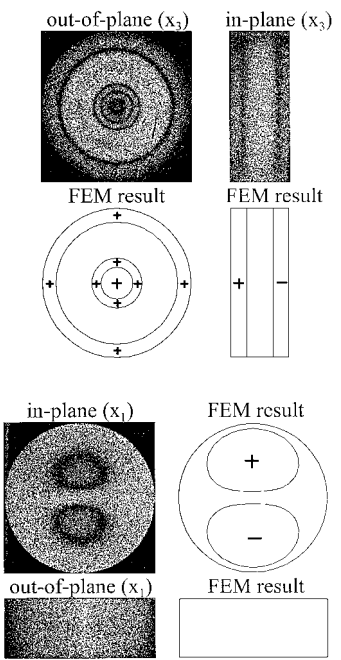**Fig. 3 Second mode shape of the circular disk obtained by AF-ESPI and FEM.**

Fig. 5 Fourth mode shape of the circular disk obtained by AF-ESPI and FEM.
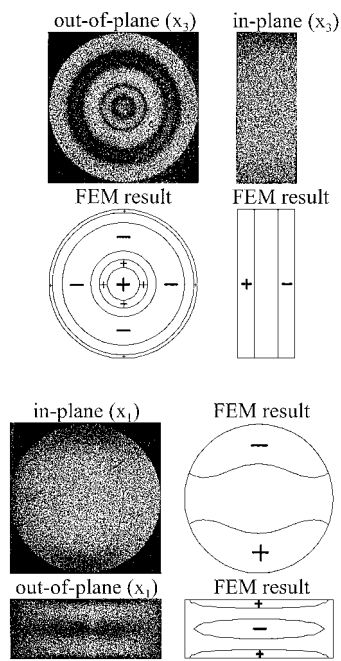

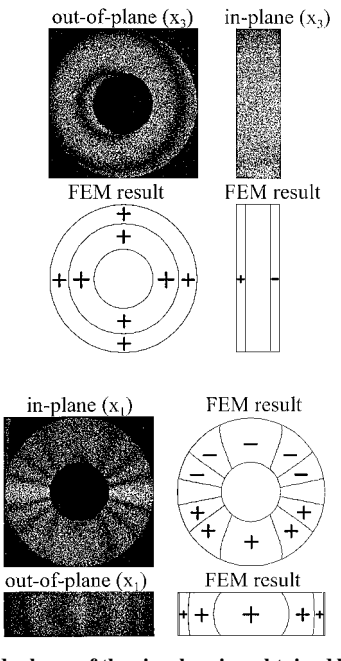**Fig. 4 Third mode shape of the circular disk obtained by AF-ESPI and FEM.**

Fig. 6 First mode shape of the circular ring obtained by AF-ESPI and FEM.

by impedance analysis and the numerical calculation will be used in the comparison with the result measured using the AF-ESPI method.

The experimental procedure of the AF-ESPI technique is performed as follows. First, a reference image is taken after the specimen vibrates, then the second image is taken, and the reference image is subtracted by the image processing system. If the vibrating frequency is not the resonant frequency, only random distributed speckles are displayed and no fringe patterns will be shown. However, if the vibrating frequency is in the neighborhood of the resonant frequency, stationary distinct fringe patterns will be observed. Then the function generator is carefully and slowly turned; the number of fringes will increase and the fringe pattern will become clearer as the resonant frequency is approached. From the aforementioned experimental procedure, the resonant frequencies and the correspondent

mode shapes can be determined at the same time using the AF-ESPI optical system. To save space here, only the first four mode shapes are presented. Figures 2–5 show the experimental and numerical results for the first four vibration mode shapes for the thick circular piezoelectric disk; both the out-of-plane and in-plane motions are shown in each mode. Note that face B in Fig. 1 represents the projection of the cylindrical surface of the disk in the view direction. Hence, it will appear as a rectangular configuration for both the experimental and numerical results. The displacement in the axial direction, i.e., x_3 direction, of the circular disk, as shown in Figs. 2–5, will be denoted as the out-of-plane motion in face A and the in-plane motion in face B. Similarly, the displacement in the x_1 direction will be denoted as the in-plane motion and the out-of-plane motion in faces A and B, respectively. Because clarity of the fringe patterns is obtained only at resonant frequencies by AF-ESPI optical measurement, we can find the resonant frequencies and the correspondent
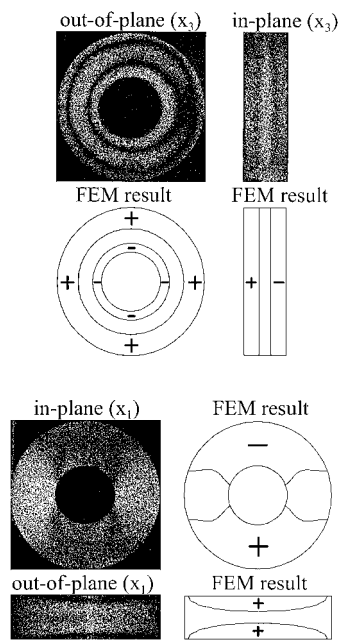
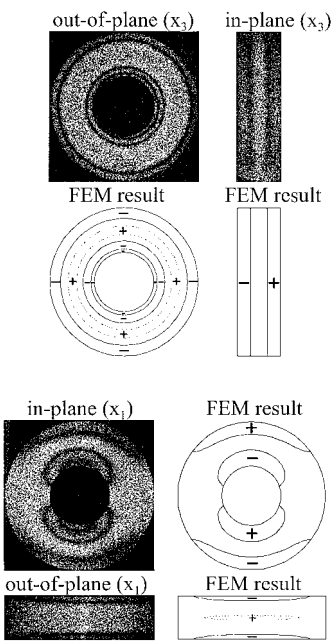**Fig. 7   Second mode shape of the circular ring obtained by AF-ESPI and FEM.**

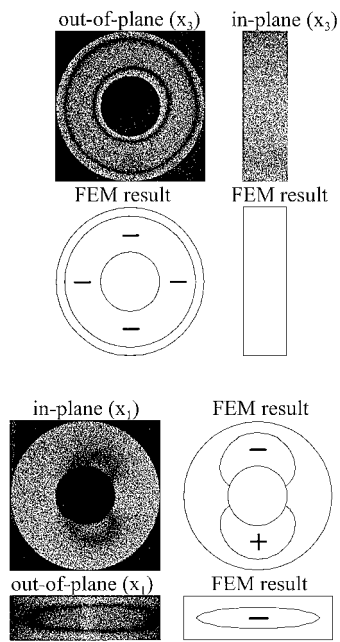**Fig. 8   Third mode shape of the circular ring obtained by AF-ESPI and FEM.**

Fig. 9   Fourth mode shape of the circular ring obtained by AF-ESPI and FEM.

Fig. 10   First mode shape of the thin-walled tube obtained by AF-ESPI and FEM.

mode shapes at the same time. As shown in Figs. 2–5, mode shapes of face A for out-of-plane (in-plane) measurement match with those of face B for in-plane (out-of-plane) measurement on the boundary between faces A and B. We can see that experimental results are in good agreement with FEM numerical calculations. We indicate the phase of displacements in the finite element results using a $+$ or $-$ sign; the regions of the same sign represent the motion in phase, and the nodal lines appear between the $+$ and $-$ signs. The amplitude of vibration mode occurring in a particular direction is relatively small if the finite element result shows a blank in the region, i.e., the in-plane motion in the x_3 direction for Fig. 2 and the out-of-plane motion in the x_1 direction for Fig. 5.

Figures 6–9 show the first four vibration modes of a thick circular ring using the AF-ESPI and the FEMs. The dashed lines shown in Fig. 9 for the out-of-plane motion in the x_3 and x_1 directions indicate that there is an out-of-phase region, but the magnitude is out of the
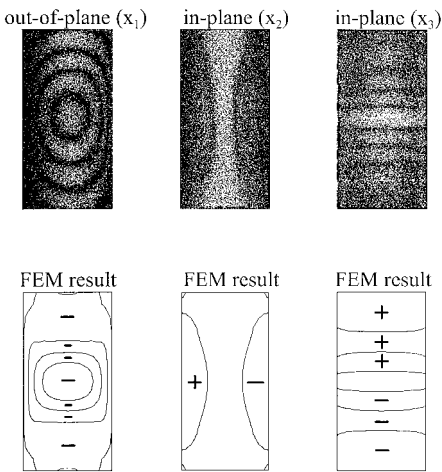
resolution for the AF-ESPI method. From the experimental fringe patterns, we can observe that the nodal lines are slightly eccentric in some modes, which means that there might be defects in the circular ring piezoelectric material due to improper manufacture process or polarization. The optical AF-ESPI method not only has the ability to measure the resonant frequencies and mode shapes but also can be applied as a nondestructive testing method to examine the quality of piezoelectric materials.

Figures 10–13 show the first four vibration modes of the thin-walled tube using experimental and numerical methods. Because we are interested in the vibration of the cylindrical surface for the thin-walled tube, three independent vibrations in each resonant frequency, i.e., two in-plane and one out-of-plane, are shown. The fringe patterns of the fourth mode in the x_1 and x_2 directions are obscure compared with those in the x_3 direction, as shown in Fig. 13. This is because displacements in the x_1 and x_2 directions are much smaller than those in the x_3 direction, which leads to the visibility of fringe patterns in the former case beyond the sensitivity of the AF-ESPI method. This also implies that the behavior of the fourth mode is dominated by the vibration in the axial direction for in-plane motion.

Table 2 Results of resonant frequencies obtained from AF-ESPI, impedance analysis, and FEM for the circular disk, circular ring, and thin-walled tube

| Mode	AF-ESPI, Hz	Impedance analysis, Hz	FEM, Hz
		Disk	
1	35,620	35,775	35,990
2	61,820	62,025	64,036
3	73,700	73,750	76,854
4	90,770	91,025	92,005
5	109,100	109,150	110,351
		Ring	
1	26,850	27,150	26,639
2	77,500	78,050	79,685
3	82,860	83,150	84,023
4	106,200	106,250	107,100
5	145,250	145,300	143,991
		Tube	
1	33,020	33,100	32,235
2	46,000	46,100	44,267
3	52,700	53,000	51,428
4	113,400	114,000	112,839
5	186,400	187,000	186,577
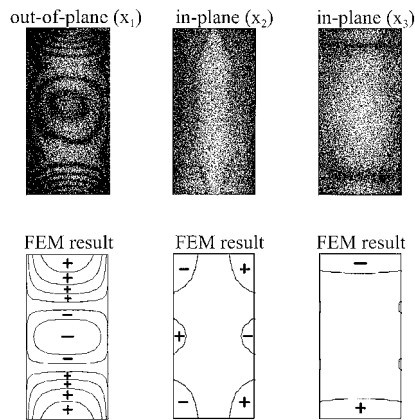
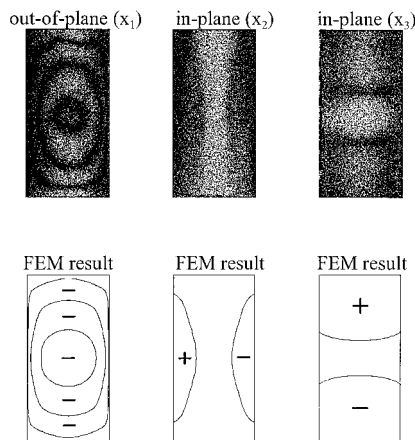Fig. 11 Second mode shape of the thin-walled tube obtained by AF-ESPI and FEM.

Fig. 12 Third mode shape of the thin-walled tube obtained by AF-ESPI and FEM.

Fig. 13 Fourth mode shape of the thin-walled tube obtained by AF-ESPI and FEM.

a)

b)

c)
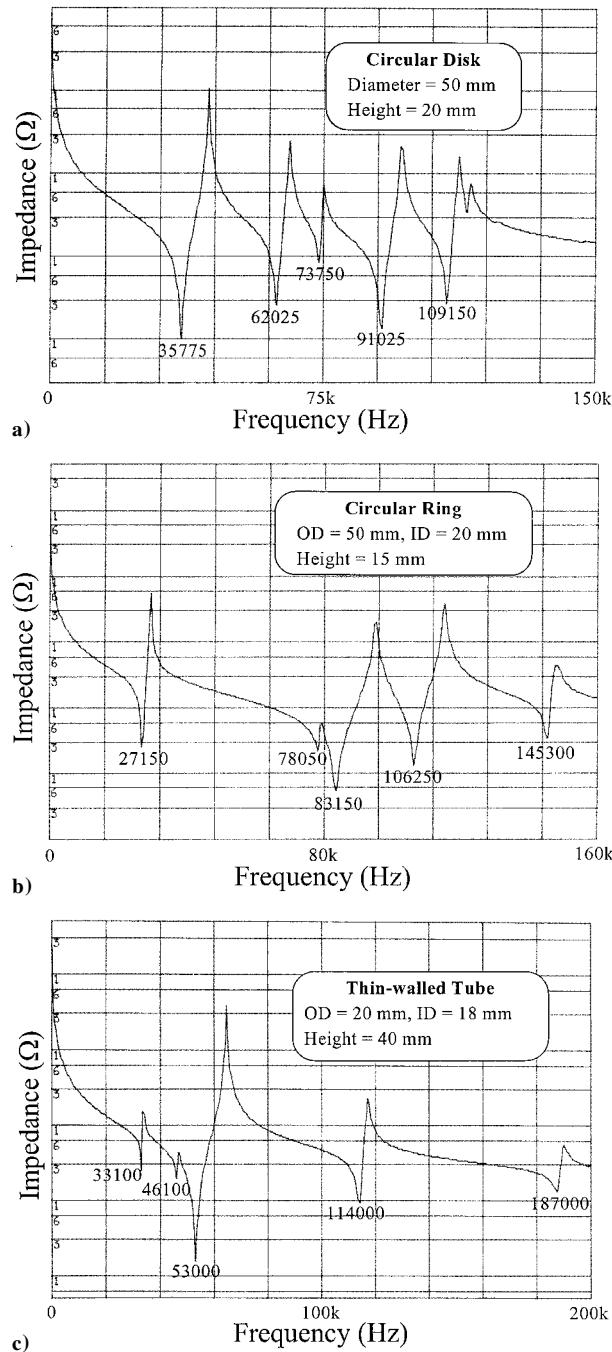
Fig. 14 Impedance curves of the a) circular disk, b) circular ring, and c) thin-walled tube.

Table 2 shows the first five resonant frequencies of the described specimens obtained using AF-ESPI, impedance analysis, and the FEM. The impedance curves for the specimens measured from HP4194A are shown in Fig. 14. The discrepancy between AF-ESPI and impedance analysis is smaller than that between AF-ESPI and FEM. However, the difference between the experimental data and FEM may be a result of the measurement of the material properties and a defect of the piezoelectric material, which is generated by the manufacturing process.
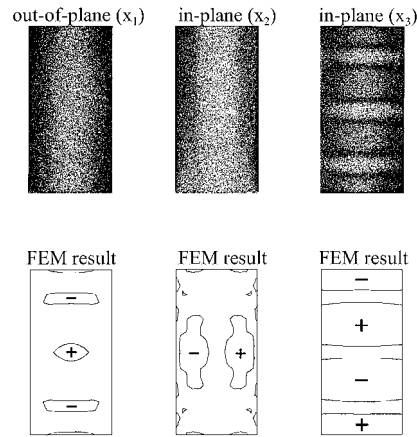
IV. Conclusions

It has been shown that the optical ESPI method has the advantages of noncontact and full-field measurement, submicron sensitivity, validity of both static deformation and dynamic vibration, and direct digital image output. The AF-ESPI method has been employed to investigate in-plane and out-of-plane vibration for three-dimensional configurations of a circular disk, a ring, and a thin-walled tube for piezoelectric ceramic material. Both in-plane and out-of-plane experimental vibration mode shapes on each face of the specimens are obtained, and the results compare very well with numerical finite element calculations. From the experimental fringe patterns, we can find that the sensitivity and resolution of the AF-ESPI method are much better than the conventional subtraction method. The resonant frequencies of the piezoelectric material are usually determined experimentally by impedance analysis. However, the resonant frequencies can also be obtained experimentally from the proposed AF-ESPI method. The resonant frequencies obtained by the AF-ESPI method are in good agreement with the impedance analysis; in addition, full-field pictures of mode shapes are also displayed at the same time using AF-ESPI. The AF-ESPI method is applicable to many situations in engineering vibration analysis for two- or three-dimensional measurement, as long as the vibration amplitude reaches the sensitivity of the AF-ESPI method.

References

[1] Rastogi, P. K., *Holographic Interferometry*, Springer–Verlag, Berlin, 1994.

[2] Butters, J. N., and Leendertz, J. A., "Speckle Pattern and Holographic Techniques in Engineering Metrology," *Optics and Laser Technology*, Vol. 3, No. 1, 1971, pp. 26–30.

[3] Jones, R., and Wykes, C., *Holographic and Speckle Interferometry*, Cambridge Univ. Press, Cambridge, England, UK, 1989.

[4] Løkberg, O. J., and Hogmoen, K., "Use of Modulated Reference Wave in Electronic Speckle Pattern Interferometry," *Journal of Physics E: Scientific Instruments*, Vol. 9, 1976, pp. 847–851.

[5] Hurden, A. P. M., "An Instrument for Vibration Mode Analysis Using Electronic Speckle Pattern Interferometry," *NDT International*, Vol. 15, No. 3, 1982, pp. 143–148.

[6] Shellabear, M. C., and Tyrer, J. R., "Application of ESPI to Three-Dimensional Vibration Measurements," *Optics and Lasers in Engineering*, Vol. 15, No. 1, 1991, pp. 43–56.

[7] Creath, K., and Slettemoen, G. Å., "Vibration-Observation Techniques for Digital Speckle-Pattern Interferometry," *Journal of the Optical Society of America A*, Vol. 2, No. 10, 1985, pp. 1629–1636.

[8] Pouet, B., Chatters, T., and Krishnaswamy, S., "Synchronized Reference Updating Technique for Electronic Speckle Interferometry," *Journal of Nondestructive Evaluation*, Vol. 12, No. 2, 1993, pp. 133–138.

[9] Wang, W. C., Hwang, C. H., and Lin, S. Y., "Vibration Measurement by the Time-Averaged Electronic Speckle Pattern Interferometry Methods," *Applied Optics*, Vol. 35, No. 22, 1996, pp. 4502–4509.

[10] Gallego-Juarez, J. A., "Piezoelectric Ceramics and Ultrasonic Transducers," *Journal of Physics E: Scientific Instruments*, Vol. 22, 1989, pp. 804–816.

[11] Zelenka, J., *Piezoelectric Resonators and Their Application*, Academia/Prague, Prague, Czech Republic, 1986.

[12] Tiersten, H. F., *Linear Piezoelectric Plate Vibrations*, Plenum, New York, 1969.

[13] Eer Nisse, E. P., "Variational Method for Electroelastic Vibration Analysis," *IEEE Transactions on Sonics and Ultrasonics*, Vol. SU-14, No. 4, 1967, pp. 153–160.

[14] Shaw, E. A. G., "On the Resonant Vibrations of Thick Barium Titanate Disks," *Journal of the Acoustical Society of America*, Vol. 28, No. 1, 1956, pp. 38–50.

[15] Kharouf, N., and Heyliger, P. R., "Axisymmetric Free Vibration of Homogeneous and Laminated Piezoelectric Cylinders," *Journal of Sound and Vibration*, Vol. 174, No. 4, 1994, pp. 539–561.

[16] Kunkel, H. A., Locke, S., and Pikeroen, B., "Finite-Element Analysis of Vibrational Modes in Piezoelectric Ceramics Disks," *IEEE Transactions on Ultrasonics, Ferroelectrics, and Frequency Control*, Vol. 37, No. 4, 1990, pp. 316–328.

[17] Guo, N., Cawley, P., and Hitchings, D., "The Finite Element Analysis of the Vibration Characteristics of Piezoelectric Disks," *Journal of Sound and Vibration*, Vol. 159, No. 1, 1992, pp. 115–138.

[18] Adelman, N. T., and Stavsky, Y., "Axisymmetric Vibrations of Radially Polarized Piezoelectric Ceramic Cylinders," *Journal of Sound and Vibration*, Vol. 38, No. 2, 1975, pp. 245–254.

[19] Adelman, N. T., and Stavsky, Y., "Vibrations of Radially Polarized Composite Piezoceramic Cylinders and Disks," *Journal of Sound and Vibration*, Vol. 43, No. 1, 1975, pp. 37–44.

[20] Chang, M., "In-Plane Vibration Displacement Measurement Using Fiber-Optical Speckle Interferometry," *Precision Engineering*, Vol. 16, No. 1, 1994, pp. 36–41.

[21] Ma, C. C., and Huang, C. H., "The Investigation of Three-Dimensional Vibration for Piezoelectric Rectangular Parallelepipeds by Using the AF-ESPI Method," *International Journal of Solids and Structures* (submitted for publication).

[22] Hibbitt, H. D., Karlsson, B. I., and Sorensen, A., "ABAQUS User's Manual," Version 5.5, Hibbit, Karlsson, and Sorensen, Inc., Pawtucket, RI, 1995.

P. R. Bandyopadhyay
Associate Editor